2013

Bearing Fault Diagnosis for Direct-Drive Wind Turbines via Current-Demodulated Signals

Xiang Gong
University of Nebraska–Lincoln, xiang.gong@huskers.unl.edu

Wei Qiao
University of Nebraska–Lincoln, wqiao@engr.unl.edu

Pages: 3419 – 3428, DOI: 10.1109/TIE.2013.2238871

Bearing Fault Diagnosis for Direct-Drive Wind Turbines via Current-Demodulated Signals

Xiang Gong, *Student Member, IEEE*, and Wei Qiao, *Senior Member, IEEE*

***Abstract*—Bearing faults account for a large portion of all faults in wind turbine generators (WTGs). Current-based bearing fault diagnosis techniques have great economic benefits and are potential to be adopted by the wind energy industry. This paper models the modulation effects of bearing faults on the stator currents of a direct-drive wind turbine equipped with a permanent-magnet synchronous generator (PMSG) operating with a variable shaft rotating frequency. Based on the analysis, a method consisting of appropriate current frequency and amplitude demodulation algorithms and a 1P-invariant power spectrum density algorithm is proposed for bearing fault diagnosis of variable-speed direct-drive wind turbines using only one-phase stator current measurements, where 1P frequency stands for the shaft rotating frequency of a wind turbine. Experimental results on a direct-drive wind turbine equipped with a PMSG operating in a wind tunnel are provided to verify the proposed fault diagnosis method. The proposed method is demonstrated to have advantages over the method of directly using stator current measurements for WTG bearing fault diagnosis.**

***Index Terms*—Ball bearings, current measurement, demodulation, fault diagnosis, frequency-domain analysis, phase-locked loops, wind energy, wind power generation.**

NOMENCLATURE

D_b	Ball diameter of a ball bearing.
D_c	Pitch diameter of a ball bearing.
θ	Ball contact angle of a ball bearing.
f_i	Characteristic frequency of an inner-race fault.
f_o	Characteristic frequency of an outer-race fault.
f_b	Characteristic frequency of a ball fault.
f_c	Characteristic frequency of a cage fault.
f_r	Shaft rotating (1P) frequency of a wind turbine.
N_B	Number of balls in a ball bearing.
t	Time index.
T	Torque of wind turbine shaft.
T_0	Torque due to variable wind power.
A_v	Amplitude of shaft torque variation.
f_{fault}	Characteristic frequency of a bearing fault (one of f_i, f_o, f_b, and f_c) in vibration measurements.
f_1	Fundamental frequency of stator current signal.
$f_{1,w}$	Component of stator current fundamental frequency signal generated by variable wind power.
$A_{1,v}$	Amplitude of component of stator current fundamental frequency signal due to a bearing fault.
φ_f	Phase of component in stator current fundamental frequency signal created by a bearing fault.
I_s	Amplitude of stator current signal.
$I_{s,w}$	Component of stator current amplitude signal generated by variable wind power.
$A_{s,v}$	Amplitude of component of stator current amplitude signal due to a bearing fault.
ψ_f	Phase of component in stator current amplitude signal created by a bearing fault.
C_s	Stator current signal.
p	Number of pole pairs in a generator.
e	Error between real and estimated stator current fundamental frequencies.
$f_{1,e}$	Estimated stator current fundamental frequency.
ϕ	Phase of current signal.
I_{dc}	Constant component of C_s^2.
I^n	High-frequency components of C_s^2.
Ω_r	Normalized frequency of f_r.
$f_{r,r}$	1P frequency of a wind turbine in a resampled current-demodulated signal.
$\Omega_{r,r}$	Normalized frequency of $f_{r,r}$.
f_s	Sampling frequency.
$f_{s,r}$	Equivalent constant sampling frequency of a resampled current-demodulated signal.
f_{base}	Expected constant 1P frequency in resampled current-demodulated signals.
l_{base}	Base value of downsampling step size.
N	Length of data.
L	Resolution of an algorithm in frequency domain.
$f_{c,\text{fault}}$	Characteristic frequency of a bearing fault in current signals.

Manuscript received April 1, 2012; revised August 25, 2012, and November 14, 2012; accepted December 18, 2012. Date of publication January 9, 2013; date of current version April 11, 2013. This work was supported in part by the U.S. Department of Energy under Grant DE-EE0001366 and in part by the Nebraska Center for Energy Sciences Research.

The authors are with the Department of Electrical Engineering, University of Nebraska-Lincoln, Lincoln, NE 68588-0511 USA (e-mail: xiang.gong@huskers.unl.edu; wqiao@engr.unl.edu).

Color versions of one or more of the figures in this paper are available online at http://ieeexplore.ieee.org.

Digital Object Identifier 10.1109/TIE.2013.2238871

I. INTRODUCTION

BEARING faults constitute a significant portion of all faults in wind turbine generators (WTGs) [1]–[3]. It is highly desired to detect bearing faults and repair or replace the faulted bearing(s) timely to prevent catastrophic damages and reduce the downtime of WTGs.

According to the types of sensor measurements used, most methods for condition monitoring of bearings in electric machines can be classified into the following categories: vibration monitoring, temperature monitoring, chemical analysis,

acoustic emission monitoring, sound pressure monitoring, laser monitoring, and current monitoring [4]. The current-based bearing fault diagnosis techniques have received more and more attention due to their advantages over other methods in terms of cost, implementation, and system reliability [5]. The current-based methods only use generator current measurements that are already used by the control systems of WTGs; no additional sensors or data acquisition devices are needed. Moreover, current signals are reliable and easily accessible from the ground without intruding the WTGs that are situated on high towers and installed in remote areas. Therefore, current-based bearing fault diagnosis techniques have great economic benefits and are potential to be adopted by the wind energy industry.

There are two main challenges of using current signals for WTG bearing fault diagnosis. First, the useful information in current signals for bearing fault diagnosis usually has a low signal-to-noise ratio. Second, it is difficult to diagnose a bearing fault in a WTG operating with a variable 1P frequency, where 1P frequency stands for the shaft rotating frequency of the WTG. Spectrum analysis algorithms have been successfully applied to current signals for bearing fault detection of electric machines running at constant speeds [6]–[9]. However, since a WTG usually operates with a variable 1P frequency, the current signals and the corresponding fault signatures in the current signals are nonstationary. Consequently, the useful information related to bearing faults easily has overlaps with the dominant components in the frequency spectra of current signals for a variable-speed WTG and, therefore, cannot be extracted directly by using traditional spectrum analysis algorithms that work for stationary signals. Time–frequency analysis algorithms are able to extract bearing fault signatures from nonstationary current measurements [10]–[13]. Nevertheless, these algorithms usually have low resolution and require high computational resources [14].

It is well known that a bearing fault will cause two effects in an induction machine: radial rotor movement and shaft torque variation [15]. A radial rotor movement leads to current amplitude modulation (AM) in an induction machine [18], [19], while a shaft torque variation leads to both current frequency modulation (FM) [10], [15] and AM in an induction machine [20]. Appropriate demodulation algorithms can separate the useful information related to a bearing fault from the dominant components of the current signals to facilitate the extraction of bearing fault signatures from the current signals. It has been proved that demodulation algorithms are able to discover bearing faults via current measurements for wind turbines equipped with doubly fed induction generators [21], [22]. However, these papers did not take into account the interferences, which are generated due to variable 1P frequencies of the WTGs, in current-demodulated signals. In other papers [23], [24], fundamental-frequency components of stator currents were used for electric machine bearing fault detection. Fundamental-frequency components are actually frequency-demodulated signals of the stator currents. However, the methods proposed in these papers were only verified for bearing fault diagnosis of electric machines operating in constant-speed conditions. Little work has been reported on bearing fault diagnosis for direct-drive wind turbines equipped with permanent-magnet synchronous generator (PMSG) operating in variable-speed conditions by using current-demodulated signals.

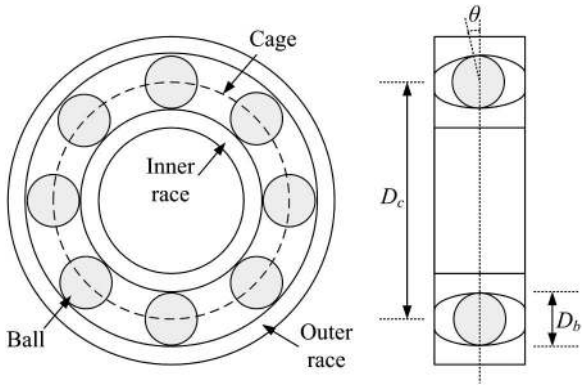

Fig. 1. Configuration of a ball bearing.

In this paper, the effects of bearing faults on the generator stator currents of a direct-drive PMSG wind turbine operating with a variable 1P frequency are modeled. The analysis using the proposed model shows that the shaft torque variation created by a bearing fault and variable wind power both modulate the amplitude and frequency of the PMSG stator current signal. Appropriate amplitude and frequency demodulation algorithms are therefore designed to facilitate the extraction of bearing fault signatures from the current signal. A 1P-invariant power spectrum density (PSD) algorithm [25] is then proposed for fault signature extraction. In the proposed algorithm, the nonstationary current-demodulated signals are resampled such that the variable 1P frequency becomes a constant value. As a consequence, the nonstationary current-demodulated signals and the corresponding fault signatures in the signals become stationary. The PSD of the resampled stationary current-demodulated signals is then calculated, from which the signatures of bearing faults can be extracted effectively for WTG bearing fault diagnosis. The proposed current-demodulation-based bearing fault diagnosis method is verified by experimental results for multiple types of bearing faults in a practical direct-drive PMSG wind turbine operating in a wind tunnel.

II. Stator Current Modulation Due to Bearing Faults

A. Types of Bearing Faults

According to the stages in the fault development process, bearing faults can be categorized into two types [26]: 1) single-point fault, which is defined as a single and localized fault on an otherwise relatively undamaged bearing surface, and 2) generalized roughness, which is a type of fault where the condition of a bearing surface has degraded considerably over a large area and become rough, irregular, or deformed.

The single-point faults in a ball bearing include the inner-race fault, outer-race fault, ball fault, and cage fault. These faults result in shaft torque vibrations of the electric machines, which modulate the current signals of the machines [15]. The characteristic frequencies of a single-point fault in vibration measurements depend on the bearing geometry and rotating frequency. The configuration of a ball bearing is shown in Fig. 1,

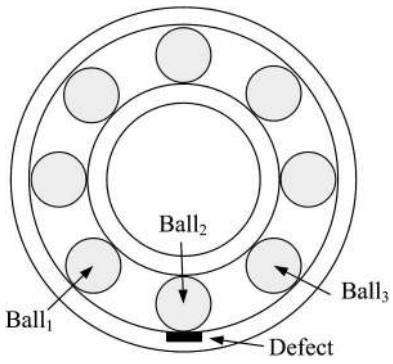

Fig. 2. Ball bearing with an outer-race fault.

where D_b is the ball diameter, D_c is the pitch diameter, and θ is the ball contact angle, which is normally zero [6]. The theoretical fundamental characteristic frequencies of the four types of single-point faults in vibration measurements are given hereinafter [27]

$$f_i = 0.5 \cdot N_B \cdot f_r \cdot \left(1 + \frac{D_b \cdot \cos\theta}{D_c}\right) \tag{1}$$

$$f_o = 0.5 \cdot N_B \cdot f_r \cdot \left(1 - \frac{D_b \cdot \cos\theta}{D_c}\right) \tag{2}$$

$$f_b = 0.5 \cdot f_r \cdot \left(\frac{D_c}{D_b}\right) \cdot \left[1 - \left(\frac{D_b \cdot \cos\theta}{D_c}\right)^2\right] \tag{3}$$

$$f_c = 0.5 \cdot f_r \cdot \left(1 - \frac{D_b \cdot \cos\theta}{D_c}\right) \tag{4}$$

where f_i is the characteristic frequency of an inner-race fault; f_o is the characteristic frequency of an outer-race fault; f_b is the characteristic frequency of a ball fault; f_c is the characteristic frequency of a cage fault; f_r is the rotating frequency of the bearing, which is equal to the 1P frequency of the WTG; and N_B is the number of balls in the bearing. Harmonics of these fundamental characteristic frequencies may also exist in vibration measurements due to bearing faults. Based on the data sheet of the bearing 7C55MP4017 used in the experiments of this paper, N_b is eight, D_c is measured to be 33 mm, and D_b is measured to be 8 mm. Therefore, if f_r is constant at 10 Hz, f_o and f_c are approximately 30.5 and 3.8 Hz, respectively.

The generalized roughness does not generate characteristic frequencies in the vibration measurements [26]. This type of bearing fault is not in the scope of this paper.

B. Radial Rotor Movement

It is reported that the effect of a radial rotor movement is negligible in an electric machine equipped with the bearings shown in Fig. 1 [24]. This is also true for direct-drive PMSG wind turbines. A bearing with an outer-race fault is shown in Fig. 2. It is assumed that, when Ball_2 passes through the fault on the outer race, a radial rotor movement will be generated in the electric machine in which the bearing is installed [15]. However, in this case, Ball_1 and Ball_3 support the inner race of the bearing, and the radial rotor movement is too small to be detectable. Moreover, a direct-drive PMSG wind turbine

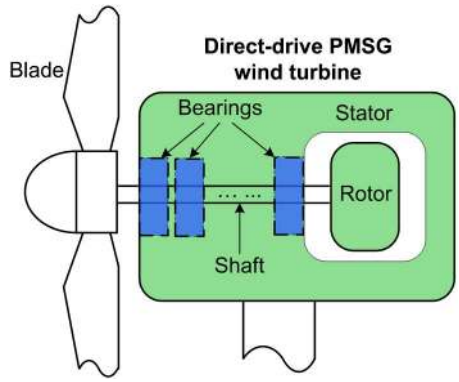

Fig. 3. Configuration of a direct-drive PMSG wind turbine equipped with multiple bearings.

usually uses more than one bearing, as shown in Fig. 3. When one of the bearings has a single-point fault, other bearings will support the shaft. In this case, the radial rotor movement and the consequent relative air gap variation are negligible. Therefore, the radial rotor movement is not considered when modeling the effects of bearing faults on generator stator current signals for direct-drive PMSG wind turbines.

C. Modulation of Stator Current Signals Due to Shaft Torque Variation

For a direct-drive PMSG wind turbine, the shaft torque generated by wind power and affected by a bearing fault when the WTG operates with a variable 1P frequency can be modeled as follows:

$$T(t) = T_0(t) + A_v \cdot \cos\left[\int 2\pi \cdot f_{\text{fault}}(t) \cdot dt\right] \tag{5}$$

where t is the time index, T is the torque on the WTG shaft, T_0 is the torque due to variable wind power, and A_v is the amplitude of the shaft torque variation created by the bearing fault. The shaft torque variation has a frequency of f_{fault}, which is the characteristic frequency of the bearing fault in vibration measurements and is one of f_i, f_o, f_b, and f_c described by (1)–(4).

It is well known that a shaft torque variation, as given in (5), leads to stator current AM and FM in electric machines [15], [28]–[30]. In a bearing fault condition, the frequency and amplitude of the modulated generator stator current signal of a PMSG wind turbine are given hereinafter

$$f_1(t) = f_{1,w}(t) + A_{1,v}(t) \cdot \sin\left[\int 2\pi \cdot f_{\text{fault}}(t) \cdot dt + \varphi_f(t)\right] \tag{6}$$

$$I_s(t) = I_{s,w}(t) + A_{s,v}(t) \cdot \sin\left[\int 2\pi \cdot f_{\text{fault}}(t) \cdot dt + \psi_f(t)\right] \tag{7}$$

where, in (6), f_1 is the fundamental frequency of the stator current signal, $f_{1,w}$ is the component of the fundamental frequency of the stator current generated by the variable wind power, and

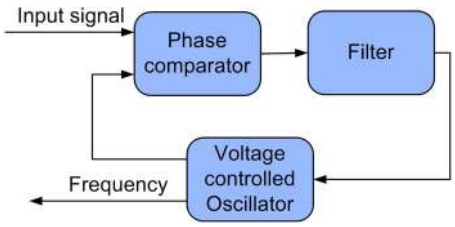

Fig. 4. Schematic diagram of a PLL for signal frequency demodulation.

$A_{1,v}$ and φ_f are the amplitude and phase of the component created by the bearing fault in the stator current fundamental frequency signal $f_1(t)$, respectively. In (7), I_s is the amplitude of the stator current signal, $I_{s,w}$ is the component of the stator current amplitude generated by the variable wind power, and $A_{s,v}$ and ψ_f are the amplitude and phase of the component created by the bearing fault in the stator current amplitude signal $I_s(t)$, respectively.

According to (6) and (7), the shaft torque variation generated by a bearing fault modulates both the frequency and the amplitude of the generator stator current signal of a direct-drive PMSG wind turbine. Thus, the fundamental frequency component of the stator current C_s can be written as

$$C_s(t) = I_s(t) \cdot \sin\left[\int 2\pi \cdot f_1(t) \cdot dt\right]. \tag{8}$$

Thereafter, in this paper, C_s is simply called the stator current. Therefore, both frequency and amplitude demodulation algorithms can be used to discover the excitations in f_1 and I_s created by a bearing fault.

III. Bearing Fault Diagnosis via Stator Current Demodulation and 1P-Invariant PSD Analysis

A. Frequency Demodulation

In a WTG, the information of the 1P frequency is usually required for maximum power point tracking control [31]. The 1P frequency is usually measured by using a position/speed sensor, e.g., an encoder or resolver, or can be estimated from the stator currents using an observer. The relationship between the 1P frequency f_r and the fundamental frequency f_1 of the PMSG stator current is given hereinafter

$$f_1(t) = p \cdot f_r(t) \tag{9}$$

where p is the number of pole pairs of the PMSG.

A simple algorithm to demodulate the frequency from a stator current signal of a PMSG is the phase-locked loop (PLL) algorithm [32], as shown in Fig. 4, where the frequency of the input signal is calculated by using a voltage-controlled oscillator.

In this paper, the input signal is the measured stator current C_s. By using the PLL algorithm, C_s is frequency demodulated to obtain the stator current fundamental frequency $f_{1,e}$

$$f_{1,e}(t) = f_1(t) + e(t) \tag{10}$$

where e is the error between the real and estimated stator current fundamental frequencies. The value of e is almost zero and can be neglected. Therefore, $f_{1,e}$ is an approximation of f_1.

The PLL algorithm has already been embedded into microcontrollers and dedicated chips [32]. Therefore, using PLL method for frequency demodulation does not require additional hardware resource.

B. Amplitude Demodulation

The square law is a classical algorithm for amplitude demodulation or envelope detection. For bearing fault diagnosis of direct-drive PMSG wind turbines, the square law is used to extract the variable amplitudes of the stator current signals. Other candidates for current amplitude demodulation include Hilbert transform and Concordia transform.

Define ϕ as the phase of the current signal C_s in (8)

$$\phi(t) = \int 2\pi \cdot f_1(t) \cdot dt. \tag{11}$$

Applying the square law to the current signal C_s yields

$$C_s^2(t) = \{I_{s,w}(t) + A_{s,v}(t) \cdot \sin\left[\int 2\pi \cdot f_{\text{fault}}(t) \cdot dt + \psi_f(t)\right]\}^2 \cdot \sin^2[\phi(t)]. \tag{12}$$

Rewrite (13) by using trigonometric identities

$$C_s^2(t) = I_{\text{dc}} + I_{s,w}(t) \cdot A_{s,v}(t) \cdot \sin\left[\int 2\pi \cdot f_{\text{fault}}(t) \cdot dt + \psi_f(t)\right] - \frac{1}{4}A_{s,v}^2(t) \cdot \cos\left[\int 4\pi \cdot f_{\text{fault}}(t) \cdot dt + 2\psi_f(t)\right] + I^n \tag{13}$$

where I_{dc} is the constant component of C_s^2 and I^n stands for the high-frequency components of C_s^2. The second component in (13) is an excitation due to the shaft torque variation created by the bearing fault. The third component in (13) is the second harmonic of the excitation in C_s^2 generated by the shaft torque variation. Since the fundamental frequency is the dominant component in the stator current signal, the amplitude of $I_{s.w}(t)$ is much larger than $A_{s.v}$. Therefore, the second harmonic of the excitation has a low magnitude and can be neglected.

C. Fault Signature Extraction

Since the shaft torque variation generated by a bearing fault leads to both FM and AM of the stator current signals, neither a frequency nor an amplitude demodulation algorithm can discover the whole effect caused by the bearing fault. To improve the accuracy of bearing fault diagnosis and increase the redundancy and reliability of the fault diagnosis system, it is recommended that both the frequency and amplitude demodulation algorithms should be applied.

Using the demodulated signals for bearing fault diagnosis has obvious advantages over directly using the stator current measurements. In bearing fault diagnosis, the major noise in the stator currents and the demodulated signals of the stator currents

are fundamental-frequency component and dc component, respectively. If a bearing fault occurs, an excitation will appear at the fault characteristic frequency f_{fault} of the frequency- and amplitude-demodulated signals, as shown in (6), (10), and (13), and can be easily separated from the dominant dc component that is irrelevant to the fault. On the other hand, there are multiple fault characteristic frequencies in the stator current measurements C_s described by (8) for all four types of single-point bearing faults due to FM and AM [15]. The excitations at these characteristic frequencies due to bearing faults could be masked by the subbands of the dominant components that are irrelevant to the faults in the frequency spectra of the current signals and, therefore, are difficult to be discovered. Furthermore, if a stator current signal is directly used for bearing fault diagnosis, the total energy of the excitations related to a bearing fault will be dispersed into multiple characteristic frequencies. Consequently, the magnitudes of the excitations at these characteristic frequencies will be lower than that at the only characteristic frequency when the frequency-demodulated signal is used.

In a WTG, in addition to the bearing fault-induced shaft torque variation, the variable wind speed also induces shaft torque variation, which will generate oscillations in $f_{1.w}$ and $I_{s.w}$ of f_1 and I_s described by (6) and (7), respectively. Therefore, an appropriate algorithm is needed to separate the bearing fault-induced shaft torque variation from the variable-wind-speed-induced shaft torque variation to extract the signatures of bearing faults contained in f_1 and I_s. Since the excitations generated by a bearing fault in the current-demodulated signals have a characteristic frequency of f_{fault}, whose value is variable and depends on the variable 1P frequency as shown in (1)–(4), a 1P-invariant PSD algorithm [25] is proposed to discover the excitations at the variable bearing fault characteristic frequency.

Define Ω_r as the normalized frequency in radians per sample of the variable 1P frequency f_r in the current-frequency- and current-amplitude-demodulated signals, and define f_s as the sampling frequency of the current measurement. The relationship among f_r, f_s, and Ω_r can be written as

$$\frac{\Omega_r(t)}{2\pi} = \frac{f_r(t)}{f_s}. \tag{14}$$

In the 1P-invariant PSD algorithm, resampling is performed such that the sampling frequency f_s changes continuously with respect to $f_r(t)$ to make the right-hand side of (14) constant. Consequently, $\Omega_r(t)$ becomes a constant value $\Omega_{r,r}$. Then, the traditional PSD analysis is applied to the resampled current-demodulated signals, in which the sampling frequency $f_{s,r}$ of the resampled current-demodulated signals is treated as a constant value. Therefore, the 1P frequency in the PSD of the resampled current-demodulated signals also becomes a constant value $f_{r,r}$, as given hereinafter

$$\frac{\Omega_{r,r}}{2\pi} = \frac{f_{r,r}}{f_{s,r}}. \tag{15}$$

Since the characteristic frequency of a bearing fault f_{fault} is proportional to f_r, as shown in (1)–(4), f_{fault} is also converted to a constant value in the 1P-invariant PSD of the current-demodulated signals to facilitate bearing fault diagnosis. The flowchart of the proposed current-demodulation-based 1P-invariant PSD algorithm for bearing fault diagnosis of direct-drive PMSG wind turbines is illustrated in Fig. 5, where only one-phase stator current signal is required. The PLL algorithm and the square law are applied for frequency demodulation and amplitude demodulation of the stator current measurements, respectively. The 1P frequency f_r of the WTG is then estimated from (9) by using the current-frequency-demodulated signal $f_{1,e}$. In the 1P-invariant PSD, the current-demodulated signals $f_{1.e}$ and C_s^2 are first interpolated with a constant ratio to ensure that the sampling frequencies of the resampled current-demodulated signals are greater than twice the f_{fault}. If the measured current is sampled with a sufficiently high sampling rate, then the interpolation is not necessary. The current-demodulated signals $f_{1.e}$ and C_s^2 are then downsampled with a variable downsampling step size of $[l_{\text{base}} \cdot f_{\text{base}}/f_r(t)]$ to convert the variable 1P frequency to a constant value, where $[\cdot]$ stands for rounding a number to the nearest integer, f_{base} is the expected constant 1P frequency in the resampled current-demodulated signals and is often chosen to be the mean value of f_r, and l_{base} is the base value of the downsampling step size, which should be large enough to eliminate the quantization error due to the requirement of an integral downsampling step size. Moreover, l_{base} should be small enough to ensure that the sampling frequencies of the resampled current-demodulated signals are greater than twice the f_{fault}. Finally, the excitations at the frequency f_{fault} in the PSD plots of the resampled current-demodulated signals are used as the signatures for WTG bearing fault diagnosis.

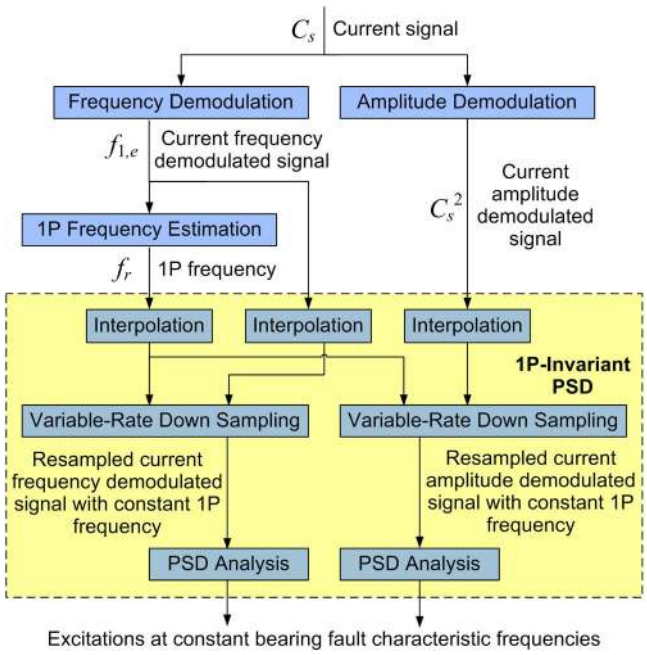

Fig. 5. Flowchart of the proposed current-demodulation-based 1P-invariant PSD algorithm for WTG bearing fault diagnosis.

D. Computational Complexity of the Proposed Algorithm

The computational complexities of the PSD analysis, wavelet analysis, and amplitude demodulation using the square law are

TABLE I
COMPUTATIONAL COMPLEXITIES OF PSD ANALYSIS, WAVELET ANALYSIS, AND AMPLITUDE DEMODULATION USING SQUARE LAW

Algorithm	Computational complexity
PSD analysis	O(N·log2N)
Continuous wavelet transform	O(N·L)
Discrete wavelet transform	O(N)
Square law	O(N)

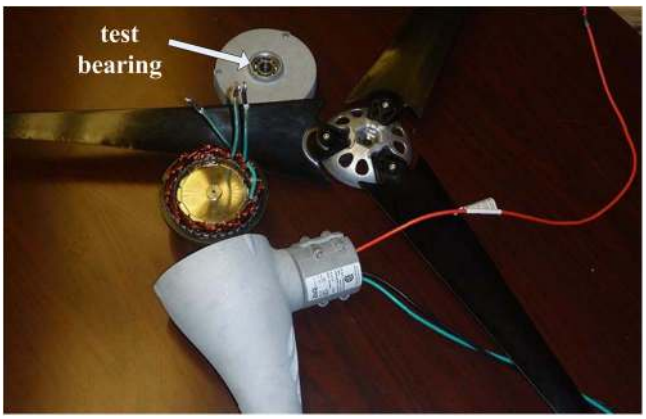

Fig. 6. Direct-drive PMSG wind turbine used in experiments.

summarized in Table I [33], [34], where N is the length of data, $\log_2$ is the logarithm to the base 2, and L represents the resolution of the algorithm in the frequency domain. If the PSD analysis and the continuous wavelet transform have the same resolution in the frequency domain, L equals N. In the proposed method, the PSD analysis and square law are applied. Therefore, the computational complexity of the proposed method is $O(N \cdot \log_2 N)$, which is smaller than that of the continuous wavelet transform. Furthermore, the computational complexity of the discrete wavelet transform is smaller than that of the proposed method. However, the resolution of the discrete wavelet transform in the frequency domain, which is approximately equivalent to that of the continuous wavelet transform when $L = 1$, is much lower than that of the proposed method.

IV. EXPERIMENTAL RESULTS

A. Experimental Setup

A 160-W Southwest Windpower Air Breeze direct-drive PMSG wind turbine was used for experimental studies, as shown in Fig. 6. The test bearing is located between the rotors of the turbine and the PMSG. The PMSG has six pole pairs. The WTG was operated in a wind tunnel, as shown in Fig. 7. The wind tunnel uses a variable-speed fan to generate controllable wind flows with the speed from 0 to 10 m/s. In the experiments, the rotating speed of the fan was adjusted to generate desired variable wind speeds in the wind tunnel. Fig. 8 shows the sensing and data acquisition system used for the test WTG in the experiments. One-phase stator current of the test WTG was recorded via a Fluke 80i-110s ac/dc current clamp. The

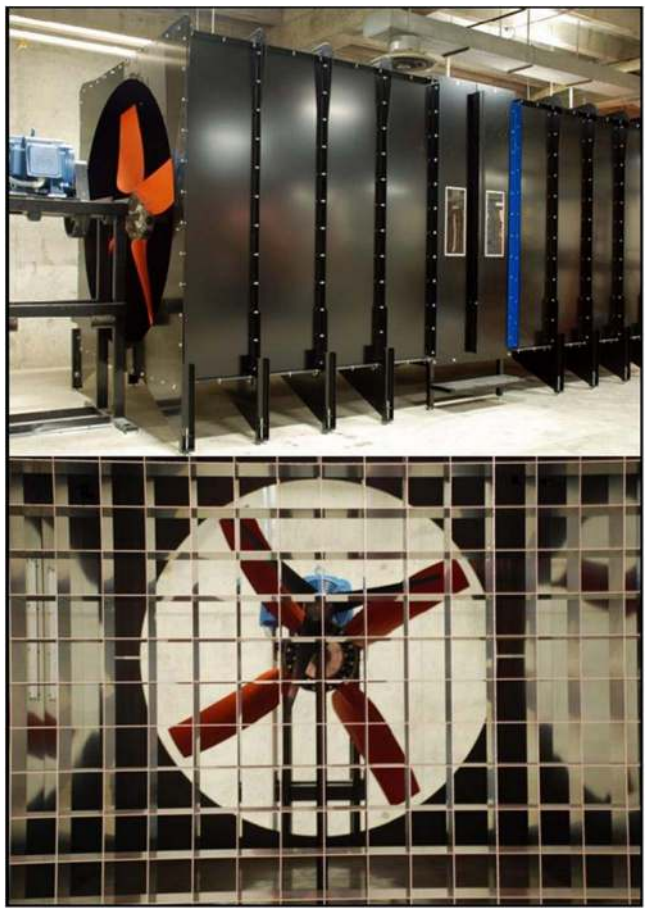

Fig. 7. Wind tunnel with the test WTG.

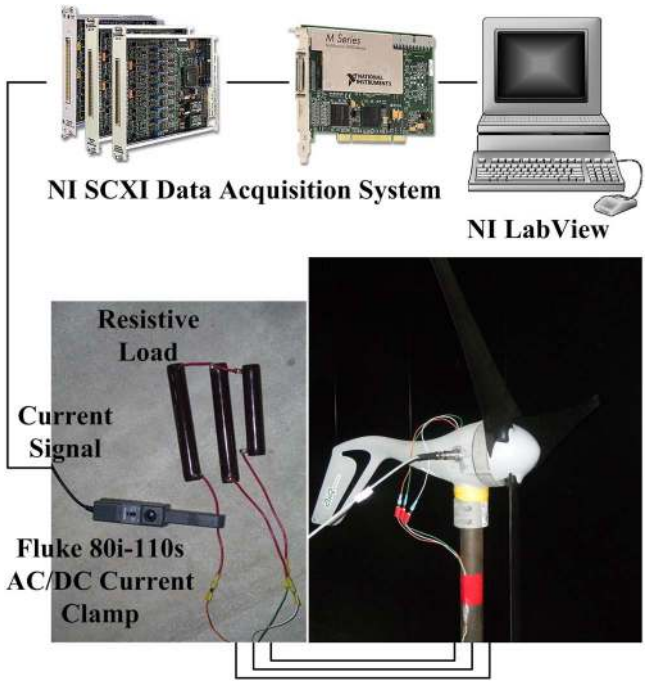

Fig. 8. Sensing and data acquisition system for the test WTG.

measured current signals were digitalized by a National Instruments data acquisition system at a sampling rate of 10 kHz. The current samples were acquired by the LabView software

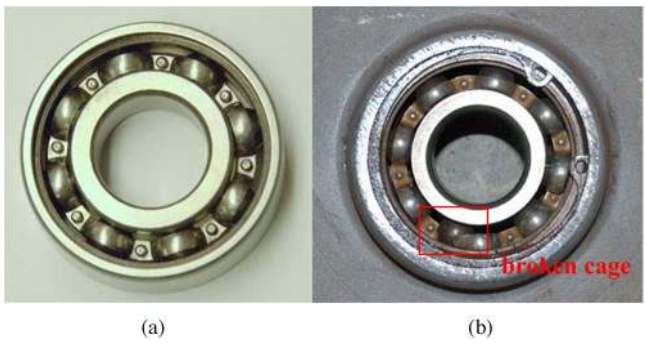

Fig. 9. Test bearing is (a) healthy before experiment and (b) with broken cage after experiment.

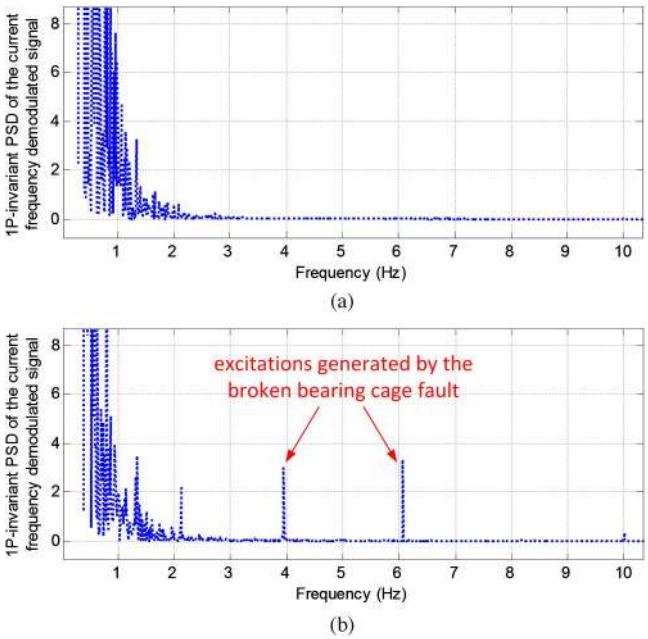

Fig. 10. Comparison of the 1P-invariant PSDs of the current-frequency-demodulated signals for the WTG with (a) a healthy bearing and (b) a broken bearing cage fault.

operating on a laboratory computer. The length of each current record is 100 s. These samples were then used for bearing fault diagnosis of the test WTG using the proposed method.

B. WTG With a Broken Bearing Cage Fault

In this test, the test bearing was pretreated by removing the lubricant oil. This accelerated the degradation of the test bearing. The WTG has been operated with a variable 1P frequency in the range of 9–12 Hz in the wind tunnel for approximately 25 h. The WTG stopped running at the end of the experiment due to the break of the bearing cage. Fig. 9 shows the test bearing before and after the experiment.

By using the proposed method shown in Fig. 5, the 1P-invariant PSDs of the frequency- and amplitude-demodulated signals of the stator current are plotted in Figs. 10 and 11, respectively, for the bearing cage fault scenario and the healthy bearing scenario. The fast Fourier transform was applied to calculate the PSD of the signals in this paper. The variable 1P frequency of the WTG was converted to a constant value of 10 Hz.

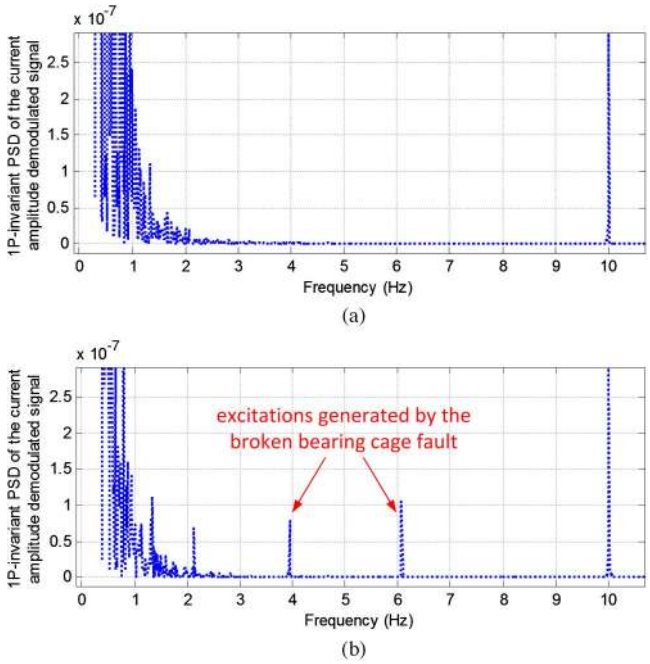

Fig. 11. Comparison of the 1P-invariant PSDs of the current-amplitude-demodulated signals for the WTG with (a) a healthy bearing and (b) a broken bearing cage fault.

In the healthy bearing scenario, no excitation appears in the range from 2 to 9 Hz in Figs. 10(a) and 11(a). However, an excitation appears at 3.95 Hz in the 1P-invariant PSD of the frequency-demodulated signal in the bearing cage fault case, as shown in Fig. 10(b). This excitation frequency is almost the same as the characteristic frequency of a bearing cage fault calculated by using (4) with the 1P frequency f_r at 10 Hz. An excitation is also found at 3.95 Hz in the 1P-invariant PSD of the amplitude-demodulated signal in Fig. 11(b) for the bearing cage fault case, as predicted by (4) and (13). These results verified that both the frequency and amplitude of the stator current are modulated by the shaft torque variation generated by the bearing fault. In addition, the 3.95-Hz bearing fault characteristic frequency and the 1P frequency f_r (10 Hz) modulate with each other and generate an excitation at 6.05 Hz $(= 10$ Hz $-$ 3.95 Hz), as shown in Figs. 10(b) and 11(b). This phenomenon has not been reported yet in any other work of current-based bearing fault diagnosis.

C. WTG With a Bearing Outer-Race Fault

A bearing outer-race fault was generated artificially for a test bearing, as illustrated in Fig. 12. The healthy bearing and the bearing with the outer-race fault were installed in the WTG and tested, respectively. The WTG operated with a variable 1P frequency in the range of 7–12 Hz in this experiment.

Figs. 13 and 14 compare the 1P-invariant PSDs of the current-frequency- and current-amplitude-demodulated signals of the WTG, respectively, for the bearing outer-race fault scenario against the healthy bearing scenario. The variable 1P frequency of the WTG was also converted to a constant value of 10 Hz. Compared to the healthy bearing scenario shown in Figs. 13(a) and 14(a), a new excitation appears at a fixed

Fig. 12. Test bearing with an outer-race fault.

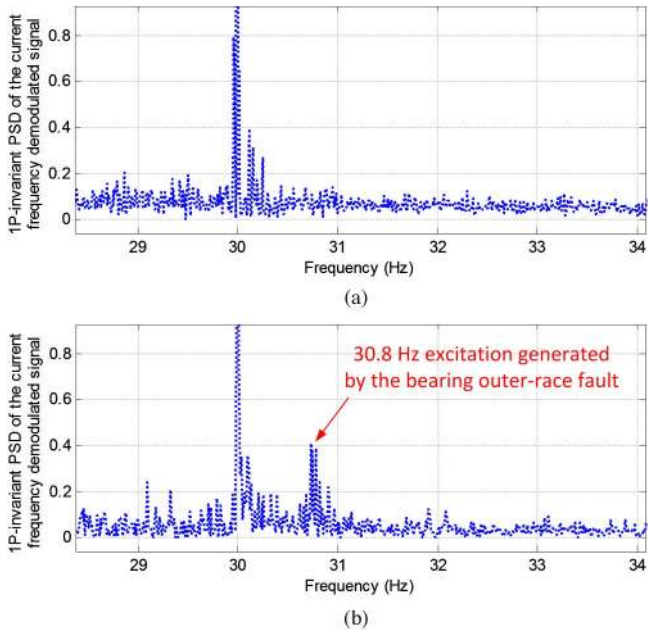

Fig. 13. Comparison of the 1P-invariant PSDs of the current-frequency-demodulated signals for the WTG with (a) a healthy bearing and (b) a bearing outer-race fault.

frequency of 30.8 Hz in the PSD plots of the bearing outer-race fault scenario, as shown in Figs. 13(b) and 14(b). This excitation frequency is almost the same as the characteristic frequency of a bearing outer-race fault calculated by using (2) with the 1P frequency f_r at 10 Hz. The magnitude of the excitation at 30.8 Hz provides an effective index for detecting and quantifying the bearing outer-race fault. These results demonstrate that the proposed method is effective for bearing fault diagnosis of direct-drive PMSG wind turbines.

D. Advantage of the Proposed Method

To illustrate the advantage of the proposed method for WTG bearing fault diagnosis, the 1P frequency of the test WTG, the traditional PSD of the stator-current-frequency-demodulated signal, and the 1P-invariant PSD of the raw stator current measurements are plotted in Figs. 15–17, respectively, for the bearing cage fault case. Fig. 15 shows that the 1P frequency of the test WTG varies continuously during the test. Because the 1P frequency is variable, the stator current fundamental frequency f_1 and the bearing fault characteristic frequency f_{fault} are both variable. As shown in Fig. 16, the excitations generated

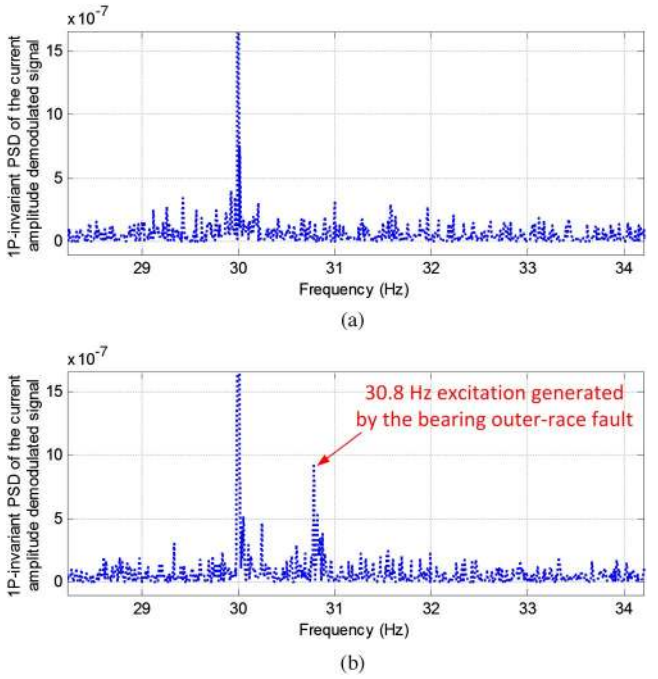

Fig. 14. Comparison of the 1P-invariant PSDs of the current-amplitude-demodulated signals for the WTG with (a) a healthy bearing and (b) a bearing outer-race fault.

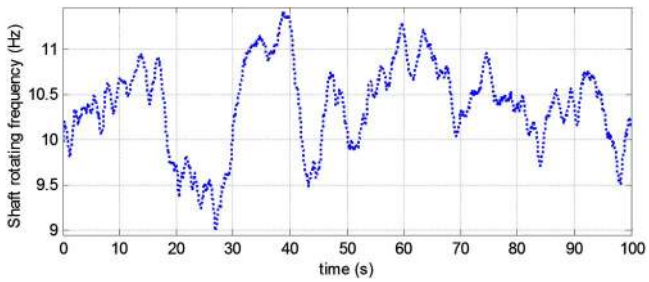

Fig. 15. Variable 1P frequency of the test WTG in the bearing cage fault case.

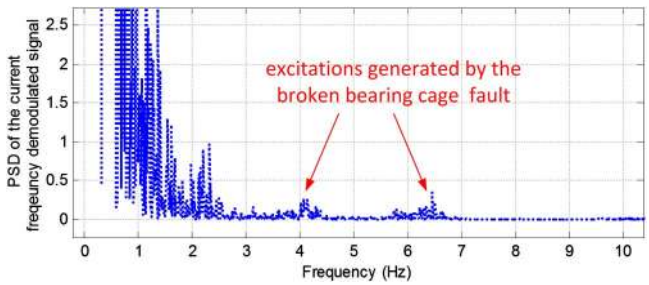

Fig. 16. Traditional PSD of the stator-current-frequency-demodulated signal in the bearing cage fault case.

by the broken bearing cage fault appear at the variable fault characteristic frequency f_c from 3.6 to 4.8 Hz and are close to the excitations in the range from dc to 3 Hz. Therefore, it is difficult to detect the broken bearing cage fault by using the traditional PSD algorithm. Based on the previous research [15], the excitations of a bearing cage fault should appear at the following frequency in current signals:

$$f_{c,\text{fault}} = f_1 \pm l \cdot f_{\text{fault}} \tag{16}$$

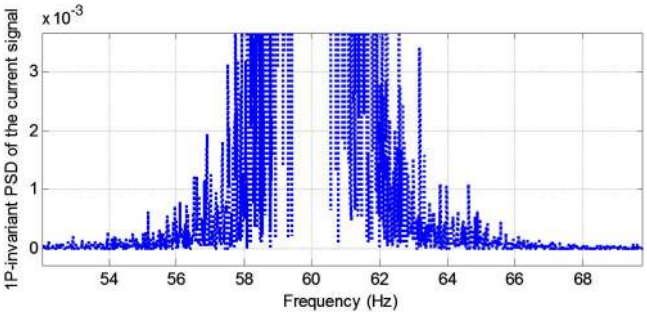

Fig. 17. 1P-invariant PSD of the raw stator current measurements in the bearing cage fault case.

where $f_{c,\text{fault}}$ is the characteristic frequency of the bearing fault in the current signals and $l = 1, 2, \ldots$. In Fig. 17, the variable 1P frequency is converted to a constant value of 10 Hz in the 1P-invariant PSD algorithm. The excitations due to the bearing cage fault should appear at $60 \pm 3.95 \cdot l$ Hz. However, these excitations are surrounded by the subbands of the fundamental frequency component due to its high magnitude. This result shows that it is difficult to identify the excitations generated by the bearing fault for the direct-drive PMSG wind turbine by using the stator current measurements directly.

V. Conclusion

This paper has analyzed and modeled the effects of bearing faults on generator stator currents of direct-drive PMSG wind turbines operating in variable rotating speed conditions. A bearing fault induces shaft torque variation in a WTG, which modulates the amplitude and frequency of the stator current signals. Based on the model and analysis, the use of current-frequency- and current-amplitude-demodulated signals has been proposed for bearing fault diagnosis of direct-drive PMSG wind turbines. However, when a WTG operates with a variable 1P frequency, the characteristic frequencies of bearing faults in the current-demodulated signals are not constant. Therefore, the signatures (e.g., excitations at the characteristic frequencies) of bearing faults may be interfered by the components created by variable WTG rotating speed in the current-demodulated signals and cannot be extracted by using traditional PSD analysis directly. To solve this problem, a 1P-invariant PSD algorithm has been proposed to discover the excitations at the characteristic frequencies of bearing faults in the current-demodulated signals. Experimental results obtained in operational environment using a wind tunnel have validated the model and the proposed method for bearing fault diagnosis of a direct-drive PMSG wind turbine. The advantages of using current-frequency- and current-amplitude-demodulated signals over directly using current signals as well as using the 1P-invariant PSD over the traditional PSD have also been demonstrated by experimental results.

The proposed method only uses one-phase stator current signal, which has been used by existing WTG control systems; no additional sensors or data acquisition devices are required. Moreover, the proposed method has high resolution and low computational cost. Therefore, the proposed method has great potential to be adopted by the wind energy industry for online condition monitoring and fault diagnosis of WTGs.

In future work, field tests will be performed for WTGs operating in real-world conditions, from which some practical issues, such as the influence of other interferences (e.g., tow vibrations), will be investigated to further validate and extend the proposed method for real-world applications.

References

[1] B. Lu, Y. Li, X. Wu, and Z. Yang, "A review of recent advances in wind turbine condition monitoring and fault diagnosis," in *Proc. IEEE Symp. Power Electron. Mach. Wind Appl.*, Jun. 24–26, 2009, pp. 1–7.

[2] Z. Daneshi-Far, G. A. Capolino, and H. Henao, "Review of failures and condition monitoring in wind turbine generators," in *Proc. XIX Int. Conf. Elect. Mach.*, Sep. 6–8, 2010, pp. 1–6.

[3] F. Napolitano, M. Paolone, A. Borghetti, C. A. Nucci, A. Cristofolini, C. Mazzetti, F. Fiamingo, and M. Marzinotto, "Models of wind-turbine main-shaft bearings for the development of specific lightning protection systems," *IEEE Trans. Electromagn. Compat.*, vol. 53, no. 1, pp. 99–107, Feb. 2011.

[4] W. Zhou, T. G. Habetler, and R. G. Harley, "Bearing condition monitoring methods for electric machines: A general review," in *Proc. IEEE Int. Symp. Diagn. Elect. Mach., Power Electron. Drives*, Sep. 6–8, 2007, pp. 3–6.

[5] W. Zhou, T. G. Habetler, and R. G. Harley, "Incipient bearing fault detection via motor stator current noise cancellation using Wiener filter," *IEEE Trans. Ind. Appl.*, vol. 45, no. 4, pp. 1309–1317, Jul./Aug. 2009.

[6] L. Frosini and E. Bassi, "Stator current and motor efficiency as indicators for different types of bearing faults in induction motors," *IEEE Trans. Ind. Electron.*, vol. 57, no. 1, pp. 244–251, Jan. 2010.

[7] A. Garcia-Perez, R. de Jesus Romero-Troncoso, E. Cabal-Yepez, and R. Osornio-Rios, "The application of high-resolution spectral analysis for identifying multiple combined faults in induction motors," *IEEE Trans. Ind. Electron.*, vol. 58, no. 5, pp. 2002–2010, May 2011.

[8] F. Immovilli, C. Bianchini, M. Cocconcelli, A. Bellini, and R. Rubini, "Currents and vibrations in asynchronous motor with externally induced vibration," in *Proc. IEEE Int. Symp. Diagn. Elect. Mach., Power Electron. Drives*, Sep. 5–8, 2011, pp. 580–584.

[9] L. Frosini, E. Bassi, A. Fazzi, and C. Gazzaniga, "Use of the stator current for condition monitoring of bearings in induction motors," in *Proc. 18th Int. Conf. Elect. Mach.*, Sep. 6–9, 2008, pp. 1–6.

[10] M. Blodt, D. Bonacci, J. Regnier, M. Chabert, and J. Faucher, "On-line monitoring of mechanical faults in variable-speed induction motor drives using Wigner distribution," *IEEE Trans. Ind. Electron.*, vol. 55, no. 2, pp. 522–533, Feb. 2008.

[11] E. C. C. Lau and H. W. Ngan, "Detection of motor bearing outer raceway defect by wavelet packet transformed motor current signature analysis," *IEEE Trans. Instrum. Meas.*, vol. 59, no. 10, pp. 2683–2690, Oct. 2010.

[12] S. J. Watson, B. J. Xiang, W. Yang, P. J. Tavner, and C. J. Crabtree, "Condition monitoring of the power output of wind turbine generators using wavelets," *IEEE Trans. Energy Convers.*, vol. 25, no. 3, pp. 715–721, Sep. 2010.

[13] K. Teotrakool, M. J. Devaney, and L. Eren, "Adjustable-speed drive bearing-fault detection via wavelet packet decomposition," *IEEE Trans. Instrum. Meas.*, vol. 58, no. 8, pp. 2747–2754, Aug. 2009.

[14] V. Choqueuse, M. E. H. Benbouzid, Y. Amirat, and S. Turri, "Diagnosis of three-phase electrical machines using multidimensional demodulation techniques," *IEEE Trans. Ind. Electron.*, vol. 59, no. 4, pp. 2014–2023, Apr. 2012.

[15] M. Blodt, P. Granjon, B. Raison, and G. Rostaing, "Models for bearing damage detection in induction motors using stator current monitoring," *IEEE Trans. Ind. Electron.*, vol. 55, no. 4, pp. 1813–1822, Apr. 2008.

[16] H. Henao, S. H. Kia, and G. Capolino, "Torsional-vibration assessment and gear-fault diagnosis in railway traction system," *IEEE Trans. Ind. Electron.*, vol. 58, no. 5, pp. 1707–1717, May 2011.

[17] S. H. Kia, H. Henao, and G. Capolino, "Torsional vibration assessment using induction machine electromagnetic torque estimation," *IEEE Trans. Ind. Electron.*, vol. 57, no. 1, pp. 209–219, Jan. 2010.

[18] M. E. H. Benbouzid, M. Vieira, and C. Theys, "Induction motors' faults detection and localization using stator current advanced signal processing techniques," *IEEE Trans. Ind. Electron.*, vol. 14, no. 1, pp. 14–22, Jan. 1999.

[19] A. M. Knight and S. P. Bertani, "Mechanical fault detection in a medium-sized induction motor using stator current monitoring," *IEEE Trans. Energy Convers.*, vol. 20, no. 4, pp. 753–760, Dec. 2005.

[20] F. Immovilli, A. Bellini, R. Rubini, and C. Tassoni, "Diagnosis of bearing faults in induction machines by vibration or current signals—A critical comparison," *IEEE Trans. Ind. Appl.*, vol. 46, no. 4, pp. 1350–1359, Jul./Aug. 2010.
[21] Y. Amirat, V. Choqueuse, M. E. H. Benbouzid, and J. F. Charpentier, "Bearing fault detection in DFIG-based wind turbines using the first intrinsic mode function," in *Proc. 14th Int. Conf. Elect. Mach.*, Sep. 6–8, 2010, pp. 1–6.
[22] Y. Amirat, V. Choqueuse, and M. E. H. Benbouzid, "Condition monitoring of wind turbines based on amplitude demodulation," in *Proc. IEEE Energy Convers. Congr. Expo.*, Sep. 12–16, 2010, pp. 2417–2421.
[23] H. Zoubek, S. Villwock, and M. Pacas, "Frequency response analysis for rolling-bearing damage diagnosis," *IEEE Trans. Ind. Electron.*, vol. 55, no. 12, pp. 4270–4276, Dec. 2008.
[24] B. Trajin, J. Regnier, and J. Faucher, "Comparison between stator current and estimated mechanical speed for the detection of bearing wear in asynchronous drives," *IEEE Trans. Ind. Electron.*, vol. 56, no. 11, pp. 4700–4709, Nov. 2009.
[25] X. Gong and W. Qiao, "Imbalance fault detection of direct-drive wind turbines using generator current signals," *IEEE Trans. Energy Convers.*, vol. 27, no. 2, pp. 468–476, Jun. 2012.
[26] J. R. Stack, T. G. Habetler, and R. G. Harley, "Fault classification and fault signature production for rolling element bearings in electric machines," *IEEE Trans. Ind. Appl.*, vol. 40, no. 3, pp. 735–739, May/Jun. 2004.
[27] C. Bianchini, F. Immovilli, M. Cocconcelli, R. Rubini, and A. Bellini, "Fault detection of linear bearings in brushless AC linear motors by vibration analysis," *IEEE Trans. Ind. Electron.*, vol. 58, no. 5, pp. 1684–1694, May 2011.
[28] M. Blodt, J. Regnier, and J. Faucher, "Distinguishing load torque oscillations and eccentricity faults in induction motors using stator current Wigner distributions," *IEEE Trans. Ind. Appl.*, vol. 45, no. 6, pp. 1991–2000, Nov./Dec. 2009.
[29] M. Blodt, M. Chabert, J. Regnier, and J. Faucher, "Mechanical load fault detection in induction motors by stator current time–frequency analysis," *IEEE Trans. Ind. Appl.*, vol. 42, no. 6, pp. 1454–1463, Nov./Dec. 2006.
[30] I. Jaksch and P. Fuchs, "Rotor cage faults detection in induction motors by motor current demodulation analysis," in *Proc. IEEE Int. Symp. Diagn. Elect. Mach., Power Electron. Drives*, Sep. 6–8, 2007, pp. 247–252.
[31] W. Qiao, W. Zhou, J. M. Aller, and R. G. Harley, "Wind speed estimation based sensorless output maximization control for a wind turbine driving a DFIG," *IEEE Trans. Power Electron.*, vol. 23, no. 3, pp. 1156–1169, May 2008.
[32] M. Kumm, H. Klingbeil, and P. Zipf, "An FPGA-based linear all digital phase-locked loop," *IEEE Trans. Circuits Syst. I, Reg. Papers*, vol. 57, no. 9, pp. 2487–2497, Sep. 2010.
[33] Y. Chang and S. Chang, "A fast estimation algorithm on the hurst parameter of discrete-time fractional Brownian motion," *IEEE Trans. Signal Process.*, vol. 50, no. 3, pp. 554–559, Mar. 2002.
[34] S. Ma and C. Ji, "Modeling heterogeneous network traffic in wavelet domain," *IEEE/ACM Trans. Netw.*, vol. 9, no. 5, pp. 634–649, Oct. 2001.

Xiang Gong (S'09) received the B.Eng. degree in electrical engineering from Huazhong University of Science and Technology, Wuhan, China, in 2006, the M.Eng. degree in electrical engineering from Zhejiang University, Hangzhou, China, in 2008, and the Ph.D. degree in electrical engineering from the University of Nebraska-Lincoln, in 2012.

His research interests include renewable energy systems, power electronics, and condition monitoring and fault detection for wind turbine generators.

Wei Qiao (S'05–M'08–SM'12) received the B.Eng. and M.Eng. degrees in electrical engineering from Zhejiang University, Hangzhou, China, in 1997 and 2002, respectively, the M.S. degree in high-performance computation for engineered systems from Singapore–MIT Alliance, Singapore, in 2003, and the Ph.D. degree in electrical engineering from Georgia Institute of Technology, Atlanta, in 2008.

He is currently the Harold and Esther Edgerton Assistant Professor with the Department of Electrical Engineering, University of Nebraska-Lincoln. His research interests include renewable energy systems, smart grids, condition monitoring and fault diagnosis, power electronics, electric machines and drives, and computational intelligence. He is the author or coauthor of three book chapters and more than 100 papers in refereed journals and conference proceedings.

Dr. Qiao is an Associate Editor of the IEEE TRANSACTIONS ON INDUSTRY APPLICATIONS. He was the recipient of a 2010 National Science Foundation CAREER Award and the 2010 IEEE Industry Applications Society Andrew W. Smith Outstanding Young Member Award.